View metadata, citation and similar papers at core.ac.uk
brought to you by CORE
provided by ScholarBank@NUS

MORPHOLOGY DEPENDENCE OF HYBRID NANOFIBERS INCOORPORATED WITH NANOPARTICLES ON ELECTROSPINNING AND POST-TREATMENT CONDITIONS

LIU YINGJUN

NATIONAL UNIVERSITY OF SINGAPORE

2008

MORPHOLOGY DEPENDENCE OF HYBRID NANOFIBERS INCOORPORATED WITH NANOPARTICLES ON ELECTROSPINNING AND POST-TREATMENT CONDITIONS

LIU YINGJUN

(B. Sci. (Hons.), Fudan University)

A THESIS SUBMITTED

FOR THE DEGREE OF MASTER OF ENGINEERING

DEPARTMENT OF MECHANICAL ENGINEERING

NATIONAL UNIVERSITY OF SINGAPORE

2008

Acknowledgements

I would like to acknowledge and express his utmost gratitude to my graduate supervisor, Professor Seeram Ramakrishna, whose ideas and support made my time as a graduate student one of the most rewarding experiences I have ever had. Without him, the idea for this unique research may have never come up.

I want to especially express my gratitude to Dr. Rajendrakumar Suresh Barhate, whose never-ending enthusiasm, support, stories and good patience were the reason I enjoyed both in lab and during tea time.

Thank you to Mr. Abhishek Kumar, Ramakrishna Ramaseshan, and Dong Yixiang, who provided the insights, ideas and criticisms when we worked together in a team. With them, I spent the most fruitful and joyful time of the past years. Especial thanks to Rama for his painstaking effort on correcting my thesis.

Thank you to the entire Nanobioengineering Laboratory who created a warm and family-like atmosphere in the cool lab.

I have special gratitude for my parents, who have always supported me and provided me with the two best role models I could ever have. The author also thank to my wife, the gift of life.

Table of Contents

Summary

Hybrid nanofibers incorporated with nanoparticles (HNIN) are very useful in several application domains. Electrospinning and electrospraying are very effective processes to fabricate nanofibers and nanoparticles, respectively. Integration of these two production processes into a single one to produce controlled-structure HNIN is a challenging task for material scientists and engineers. The principal difficulty is bead-fiber transition during processing, which is easy to be triggered by tuning rheological properties of solution, as well as processing conditions. The second difficulty is morphology control of nanofibers and nanoparticles, which highly depends on the evaporation, sorption and swelling during post-treatment. In the present work, the bead-fiber transition conditions are initially investigated in the parameter space of concentration, molecular weight, applied voltage, conductivity, surface tension and viscosity. The bead-fiber transition is explained by Deborah number. Then the formation and evolution of the skin of nanofibers\nanoparticle during evaporation is analyzed from a physicochemical point of view, and the morphology dependence on volatility of solvent is given by the second characteristic number: skinning number. Finally the morphology of nanofibers is tailored by sorption and swelling of vapor, and beads are successfully introduced to nanofibers. The bead growth is related to the third characteristic number: beading number. By tuning the three characteristic numbers, HNIN of well-controlled morphologies are obtained.

List of Figures

List of Tables

List of Abbreviations

a	size of solvent molecule
a^3J	volumetric evaporation current
b	thickness of skin
Be	beading number
Bi	Biot number
c	molar concentration
c_e	entanglement concentration of polymeric solution
c^*	chain overlap concentration of polymeric solution
Ca	capillary number
$D(\psi)$	diffusion coefficient of solvent in the glassy skin
D_1	initial midpoint diameter of fluid filament
$D_{mid}(t)$	midpoint diameter of fluid filament at time t
$D_g(T)$	diffusivity of solvent vapor in air at temperature T
De	Deborah number
DMF	N,N-dimethyl formamide
E_s	stretching energy per unit area of skin
E_b	bending energy per unit area of skin
EHD	electrohydrodynamics
G	elastic modulus of fluid filament
HNIN	hybrid nanofibers incorporated with nanoparticles
J	evaporation current of solvent from skin outwards
k_c	mass transfer coefficient under Stokes flow
kV	kilo volts
l	characteristic length of skin
L	relative initial elongation of polymer chain in bead
m	molecular mass of solvent
mM	millimolar per liter
p_g	partial pressure of solvent in air
$p_v(T)$	vapor pressure of solvent at temperature T
PDDPPDH	potassium O, O-didodecylphosphorodithioate
PSF	polysulfone
q	charge
q_R	charge of Rayleigh limit
r_0	characteristic length
Re	Reynolds number
S	retardation number
Sc	Schmidt number
Sk	skinning number
t	thickness of diffusion layer inside the gas over the skin
t^*	characteristic time by which ω_{max} was rendered dimensionless

wt%	weight percentage
Y	Young's modulus of skin
ζ	magnitude of out-of-plane displacement
$[\eta]$	intrinsic viscosity of polymeric solution
θ	contraction ratio of skin during drying
λ	mean free path of solvent in air at atmospheric pressure
λ_p	relaxation time of polymeric solution
μ_s	viscosity of solvent
ρ	density of polymeric solution
σ	surface tension of polymeric solution
τ	ratio of the initial elastic modulus to the capillary pressure
υ	characteristic viscosity of fluid filament
υ_{th}	thermal velocity of solvent molecule
φ	volume fraction filled with the polymer chains in bead
ψ	volume fraction of solvent in nanofiber
ψ_u	volume fraction of solvent just below skin
ψ^*	critical volume fraction of solvent at glass transition
ω_{max}	maximum dimensionless growth rate of viscoelastic jet

Chapter 1 General Introduction

In this chapter, the motivation for this research is described with information about the organization of the thesis

1.1 Motivation

Hybrid nanofibers with incorporated nanoparticles (HNIN) are of great interest in materials science due to the combination of the properties of polymer fibers, such as a high aspect ratio and specific surface area, light weight, and high flexibility, with the properties found in nanoparticles, such as high chemical reactivity, size and surface effects, and magnetism. Potential applications of nanofibers of this kind include reinforcement of elastomers and plastics, catalyst supports, filtration membranes, electrodes for lithium batteries and solar cells, anisotropic optical materials, sensors, scaffolds for tissue engineering, medical implants, and supports for protein immobilization.

There has been increasing interest in the use of electrohydrodynamics (EHD) to manufacture micro- and nano-scale architectures such as fibers, particulates, and vesicles. A large amount of organic, inorganic, and hybrid (organic-inorganic) materials have been produced through two major EHD approaches: electrospinning and electrospraying. Normally, electrospinning gives uniform fibers, whereas electrospraying produces spherical particulates. Thus, integration of electrospinning and electrospraying has great industrial significance for

production of HNIN: the fabrication of nanofibers and aggregation of inorganic nanoparticles with nanofibers as templates or connectors in one step.

In order to achieve a robust integration system, I have used similar equipments for electrospinning and electrospraying processes, consisting of a solution delivery system, a pendent drop with Taylor cone meniscus, a high electric field, and a grounded collector. Based on the processing parameters and solution properties including concentration, molecular weight, applied voltage, conductivity, surface tension and viscosity, I control the bead-fiber transition to produce fibers or particulates as needed. Also I have obtained different morphologies of fibers or particulates by changing solvents of different volatility, and absorbing vapor after blending surfactant.

1.2 Thesis organization

The remaining chapters of this thesis are organized as follow. The next chapter is a survey of related works. Chapter 3 investigates the conditions of bead-fiber transition during electrospinning in the parameter space of concentration, molecular weight, applied voltage, conductivity, surface tension and viscosity. Once the nanofiber is collected, its morphology also depends on the evaporation of solvent, which will be discussed in Chapter 4. Chapter 5 investigates the bead growth on nanofibers induced by surfactant. Finally, the conclusion and future recommendations are stated in Chapter 6. .

Chapter 2 Related Works

In this chapter, several related works about controlling structure and morphology on HNIN will be described.

2.1 A brief history of electrospinning and electrospraying

The phenomenon of electrospraying has been investigated for a long time. In 1750, French clergyman and physicist Jean-Antoine Nollet reported the earliest known reference to electrospraying, over two hundred years before the term was coined. He demonstrated that water flowing from a vessel would aerosolize when the vessel was electrified and placed near electrical ground. In the early twentieth century, refined experimental techniques allowed for a more rigorous understanding of electrostatics and electrodynamics.

In 1882, Lord Rayleigh first considered the electrical pressure resulting from excess charge q on a droplet of spherical radius r and surface tension σ. His theory predicts that the natural quadrupolar oscillation of a droplet in a field-free environment becomes unstable when q exceeds the limit q_R, now known as the "Rayleigh limit", defined in the equation, $q_R = 8\pi\varepsilon^{1/2}\sigma^{1/2}r^{3/2}$. The limit is reached either by evaporation or by application of charge in excess of q_R. At $q \geq q_R$, Rayleigh postulated that the droplet would throw out liquid in fine jets [1].

John Zeleny classified the formation of ethanol electrosprays by taking photographs [2]. In his work the sprays are liquid drawn into a conical shape before

breaking into a fine mist of droplets. This work was followed by rigorous studies of the field-dependent deformation of soap films over cylindrical tubes by Wilson and Taylor. The conical shape of these films resembled Zeleny's observations of ethanol and indeed has come to be termed the Taylor cone based on later theoretical work by G. I. Taylor [3,4].

By the middle of the twentieth century, electrospraying had become a popular painting technique. Reports by Hines [5], Tilney and Peabody [6], and several patents demonstrate the ease with which paint is atomized and applied to vehicles, housewares, and various metal goods. However, it was not until 1968 that electrospraying was introduced as a scientific tool. Dole and coworkers transferred high molecular weight polystyrene ions into the gas phase from a benzene/acetone solution [7].

In the 1980's, Fenn and coworkers presented a series of papers that permanently established electrospraying as a tool to introduce dissolved large biomolecules and polymers into the gas phase. Their work attracted significant attention through spraying compounds of ubiquitous scientific interest including low molecular weight cationic clusters [8], negative ions [9], polyethylene glycol [10] and several biomolecules [11].

Electrospinning has its basis in early electrospraying studies. The first patents for obtaining fibers from a jet of material injected into a space with strong electric field were awarded to Cooley and Morton [12,13] in 1902, but the first real success

was attained in 1930, when Formhals [14] suggested that the fibers be generated from solutions of polymer resins. This method was developed in 1936 by Norton [15] for obtaining fibers from melts and solutions of rubber and other synthetic resins, however, all these patents did not lead to the production of usable fibers because of the low quality and inability to compete with commonly used fibers.

A decisive breakthrough in development and application of the electrospinning method was attained in 1938 in the USSR by N. D. Rozenblum and I. V. Petryanov-Sokolov [16]. They unexpectedly obtained strong continuous fibers with stable cross section having a diameter of the order of several microns and less, when they experimented with solid, spherical, uniformly-sized aerosol particles of nitrocellulose from its solution in acetone by the electrodynamic atomization method. Setting on a grounded electrode or on poorly insulated surfaces, they formed thin, but rather strong anisotropic layers with a quasi-uniform random fibrous structure and rather low, 2-5% volumetric packing density, highly compressed by electrical forces.

In the 1970s, Simm et al. [17] patented the production of fibers with diameters of less than 1 μm. However, this work, which was followed by other patents, also remained unnoticed. Electrospun fibers were first commercialized for filter applications, as part of the nonwoven industry [18].

Electrospinning gained substantial academic attention in the 1990s, which was partially initiated by the activities of the Reneker group [19]. One reason for the

fascination with the subject is the combination of both fundamental and application-oriented research from different science and engineering disciplines. These research efforts usually target complex and highly functional systems, which could certainly be applied on a commercial level. Fiber systems in which the macroscopic properties (that is, specific chemical, physical or biological combinations of properties) can be targeted through modifications on the molecular level are of particular interest.

2.2 Working medium

Examples of fluids suitable for electrospraying and electrospinning include molten pitch, polymer solutions, polymer melts, polymers that are precursors to ceramics, and/or molten glassy materials. A variety of fluids or materials besides those listed above have been used to make fibers including pure liquids, solutions of fibers, mixtures with small particles and biological polymers. A review and list of materials used to make fibers are described in a US patent [20], and Huang et al.. [21] gave a list of materials/ solvent that can be used to produce the nanofibers.

2.3 Bead-fiber transition

Fundamentally, electrospinning and electrospraying of polymer solutions are identical processes with an obvious difference—electrospinning results in fibers whereas electrospraying generates droplets/beads. Experience suggests that an transition between bead and fiber can be achieved by changing polymer

concentration and\or molecular weight, with morphology of products that: (1) beads only, (2) beads with incipient fibers, (3) beaded fibers, (4) fibers only and (5) globular fibers/ macrobeads [22].

2.3.1 Instabilities

During the fiber/bead formation, instability exists in two effects: (i) capillary wave breakup (Rayleigh instability) and (ii) breakage of the fiber due to the stresses overcoming some limiting tensile strength (cohesive, brittle fracture). The solution is spinnable when there are sufficient forces holding the jet together to overcome the capillary instability (lower spinnability limit). On the other hand, sufficient relaxation time (or low enough strain rates) is necessary for the material to behave in a viscoelastic manner and avoid fracture (upper spinnability limit). Nevertheless, there is an optimum range of the stabilizing forces, between which the jet is prevented from breaking into droplets (Rayleigh instability) while avoiding fracture [22].

2.3.2 Chain entanglements

Experimental observations in electrospinning confirm that for fiber formation to occur, a minimum polymer concentration is required. Below this critical value, application of voltage results in electrospraying or bead formation primarily due to a Rayleigh instability. Gupta et al. [23] and Jun et al. [24] have investigated the effect of molecular weight on continuous fiber formation at a given polymer

concentration. The importance of viscoelasticity for fiber formation was clearly demonstrated [25,26] with a fundamental assumption of the presence of an elastically deformable entanglement network. The link between the formation of entanglements in solution and their electrospinnability also has been established previously [22,27-29]. Increased chain entanglements and longer relaxation times, a consequence of increased polymer concentration and molecular weight, were thought to be responsible for fiber formation.

Stephens et al. [30] employed real time Raman spectroscopy on an ejected jet to determine the polymer/solvent ratio as a function of distance from the nozzle. They concluded that at approximately 1 cm from the nozzle tip, the polymer/solvent ratio of the ejected jet remains essentially unaltered from the initial ratio in the syringe, even volatile solvent tetrahydrofuran was employed. Consequently, the polymer concentration is not changed much. Presumably, further away from the tip as the solvent evaporates, a considerable increase in polymer concentration, entanglements and elongational viscosity occurs, thereby affecting the viscoelastic properties. These results suggest that solution properties such as polymer concentration and molecular weight significantly affect fiber/bead formation in comparison to other governing parameters (i.e. surface tension and conductivity); however, for modeling the jet and resulting fiber diameter, the other governing parameters have been shown to be significant contributions.

Larsen et al. [31] showed a control morphology transition from fibers to beaded fibers or particles without changing the operating voltage or electric current. It was achieved by using a nozzle consisting of two coaxial capillary tubes. The inner tube delivers the working solution, while the outer delivers a controlled flow of an inert gas saturated with the corresponding solvent of the solution. At a high gas flow rate, electrospray-derived particles are obtained. When the gas flow rate decreases, most droplets and some beaded fibers are collected. If it decreases even more, only beaded fibers are collected. If a jacket gas with high ionization potential is used, the suppression of corona discharges that might otherwise occur when processing aqueous systems with very high voltages are typically needed to form Taylor cones.

For this entanglement to happen, the polymer should be above a critical polymer concentration or molecular weight. However, the presence of entanglements is a sufficient but not a necessary condition for the polymer fluid to demonstrate strong elastic properties. The elastic response can also be achieved at lower polymer concentration if the relaxation time of the fluid is longer than the time of extensional deformation. This kind of elastic behavior is typical of Boger fluids that show high elasticity at concentrations well below c* [32,33]

2.4 Evaporation

A cartoon of the electrospinning and electrospraying process is shown in Figure 1.1. Here a polymer solution is pumped through a capillary needle. A high voltage

source establishes an electric field between the needle and a plate. Sufficiently high voltages produce strong fields within the solution itself drawing the liquid to a tip as it exits the needle. From this tip, the charged solution jets outward and accelerates in the electric field toward the plate.

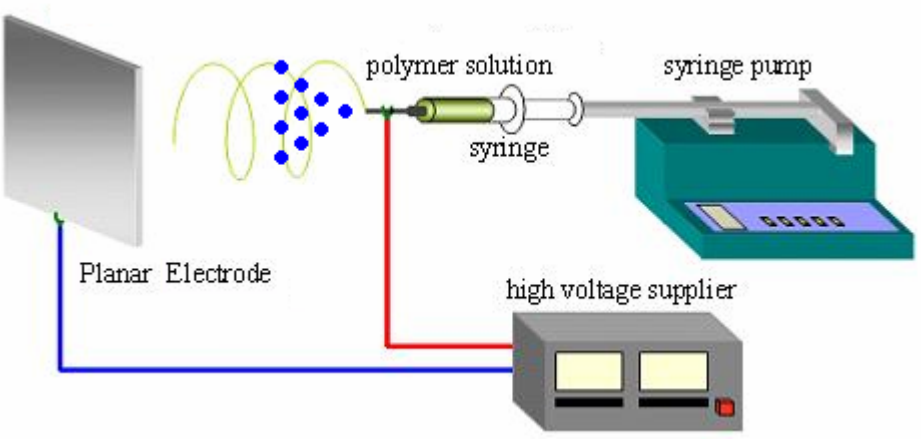

Figure 1.1 Schematic illustration of electrospinning/electrospraying device.

Despite the widespread popularity of electrospinning and electrospraying, questions remain regarding the mechanism by which the charged jet evaporates to ultimately produce fiber and\or particle form. A more thorough understanding will certainly lead to more efficient fabrications and further unique applications.

Figure 1.2 highlights the current understanding of the "life" of an evaporating charged jet. Initially, nascent jet evaporates, losing solvent molecules but not charge. As a result, the surface charge density increases to a point at which the force of Coulomb repulsion at the surface overcomes the cohesive force of surface tension. The jet releases charge and mass in a concerted "Rayleigh discharge" named after Lord Rayleigh who first predicted the event [1]. Smaller jets release

charge by a mechanism alternatively described by the ion evaporation model and the charge residue model. From there, nanoclusters of solvent and polymer might undergo even further evaporation yielding desolvated gas-phase ions.

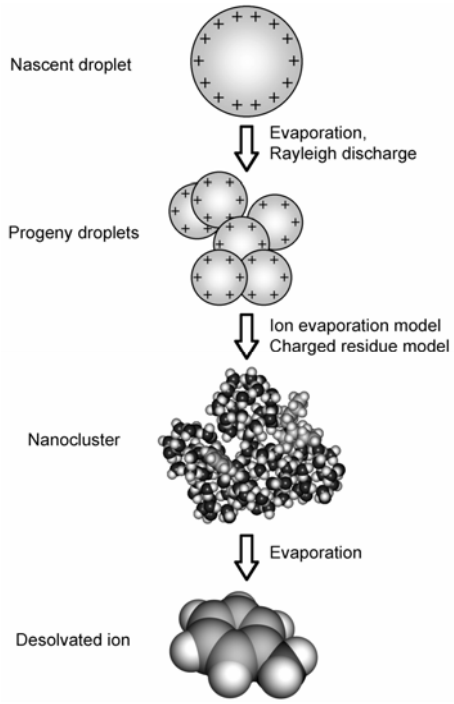

Figure 1.2. Schematic representation of the “life” of an evaporating, charged jet

Many efforts have been reported in the literature for electrospinning and electrospraying HNIN. Controlling structure and morphology is one of the most important tasks for the effective HNIN. So the morphology dependence of HNIN of electrospinning and post-treatment conditions shall be discussed in the following chapters.

Chapter 3 Bead-fiber Transition on Nanofibers Morphology

3.1 Introduction

The structure fabricated by electrospinning ranges from particulates (in which case the process may also be referred to as "electrospraying") to fibers depending on various conditions [34]. In between these extremes, a combination of these morphologies may result in beaded fibers [35], which are often considered as structural defects. As attractive features of electrospinning, these structures may also exhibit wide variations in their shapes and surface morphologies. The ultimate goal in electrospinning is to obtain the structures and morphologies of interest based on the understanding how it happens.

Some of the recent studies have focused on the transition of these structures, namely the bead-fiber transition, with respect to the rheological properties of polymer solutions. McKee et al. [28] and Gupta et al. [23] investigated morphological transitions based on critical hydrodynamic concentrations, i.e., the entanglement concentration (c_e) and the chain overlap concentration (c^*), respectively. Their results indicate that stable fibers start to form for solutions in the semi-dilute-entangled regime. Shenoy et al. [22] employed a semi-empirical approach in establishing a model for bead-fiber transition based on chain entanglement analysis. According to their model, the minimum requirement for

the formation of some fibers is one entanglement per polymer chain, whereas more than 2.5 entanglements per chain may be required to form bead-free fibers.

While the importance of chain entanglements has been recognized, other solution properties are also known to play an important role in determining the morphology of electrospun polymers [35-37]. For instance, it is well known that a solution with a high charge density results in a fine fiber structure due to the large extensional force in a jet of solution [38]. Since the solvent used determines solution properties to a large extent, several investigators have explored the change in morphology of polymers electrospun from various solvents [36-43]. Some of the reports have shown that the use of solvents with a large dielectric constant and electrical conductivity typically results in increased uniformity and reduced number of beads in the electrospun fibers [39,42,43]. The addition of salts [34,35] and surfactants [44] is also known to demonstrate a similar effect. However, a quantitative study of these parameters remains difficult as the effect of solvent properties cannot be isolated.

The influences of these numerous solution properties, including shear viscosity, polymer concentration, solution conductivity, and surface tension, on fiber morphology have been investigated experimentally [23,24,35,42]. Although researchers have recognized the important role of elastic response in electrospinning [29,45-48], its impact on the fiber morphology has not been studied systematically due to the difficulty of maintaining other solution properties constant while changing the

elasticity. In a study by Theron et al., the fluid relaxation time was measured [47]. Gupta et al. used the dimensionless quantity c[η] (where c is the polymer concentration in solution and [η] is the intrinsic viscosity) to describe fluid elasticity, and studied the formation of electrospun fibers in three different concentration regimes (dilute, semi-dilute, concentrated) [45]. In this chapter, we present a study of several series of polymer solutions showing the bead-fiber transition during electrospinning by changing the degrees of elasticity response under different concentration, molecular weight, applied voltage and conductivity.

3.2. Experimental section

3.2.1 Materials and measurement

Polysulfone with a molecular weight 26,000 g mol^{-1} was obtained from Aldrich and used without further purification. *N*,*N*-dimethyl formamide (DMF), was used as received from Aldrich. The polysulfone solution used DMF as the solvent, and the concentration of polysulfone was in the range of 10–25 wt%. The anionic surfactant potassium O, O-didodecylphosphorodithioate (PDDPPDT) was synthesized in two straightforward steps as illustrated. The reaction of 1-dodecanol with phosphorus pentasulfide gave acid, which was converted with K_2CO_3.

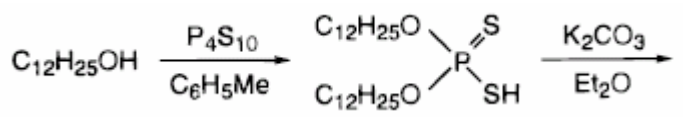

And then it was purified and characterized using H^1 NMR.

The surfactants were dissolved separately into the polymer solutions, the concentration ranging from 0.03 to 30 mM for anionic surfactants.

The viscosities and conductivities of the polymer solution were determined by a digital rotational viscometer (LV1 Brookfield) and a conductivity meter (MP220 Mettler-Toledo), respectively. The surface tension was measured by the Du Nouy Ring method, using a platinum ring (Cole Parmer) and a highly precise electronic balance (XT220A Precisa). The morphology of the electrospun fibers was observed under a field emission scanning electron microscope (FE-SEM, Quanta 200F).

3.2.2 Electrospinning

The electrospinning apparatus included a high voltage power supply (ES30P, from Gamma High Voltage Research), a syringe pump (Aldrich) and some accessories. A high voltage was applied to the polymer solution by connecting the electrode with the metal syringe needle. A grounded aluminium sheet was placed about 15 cm away from the tip of the needle. The electrospinning was conducted under the temperature range of 20-25 ℃, and at 1 kV/cm of applied electric field and a polymer flow rate of 1 ml/h, except where specifically indicated.

3.3 Results

3.3.1 Concentration effects on bead-fiber transition

Upon electrospinning polysulfone solutions, beads-only, bead-on-fiber, beads-free structures emerged in the spun fibers. As shown in Figure 3.1, the morphological transition from bead-only to bead-free structure takes place gradually over a range of polymer concentrations between 10 and 25 wt %.

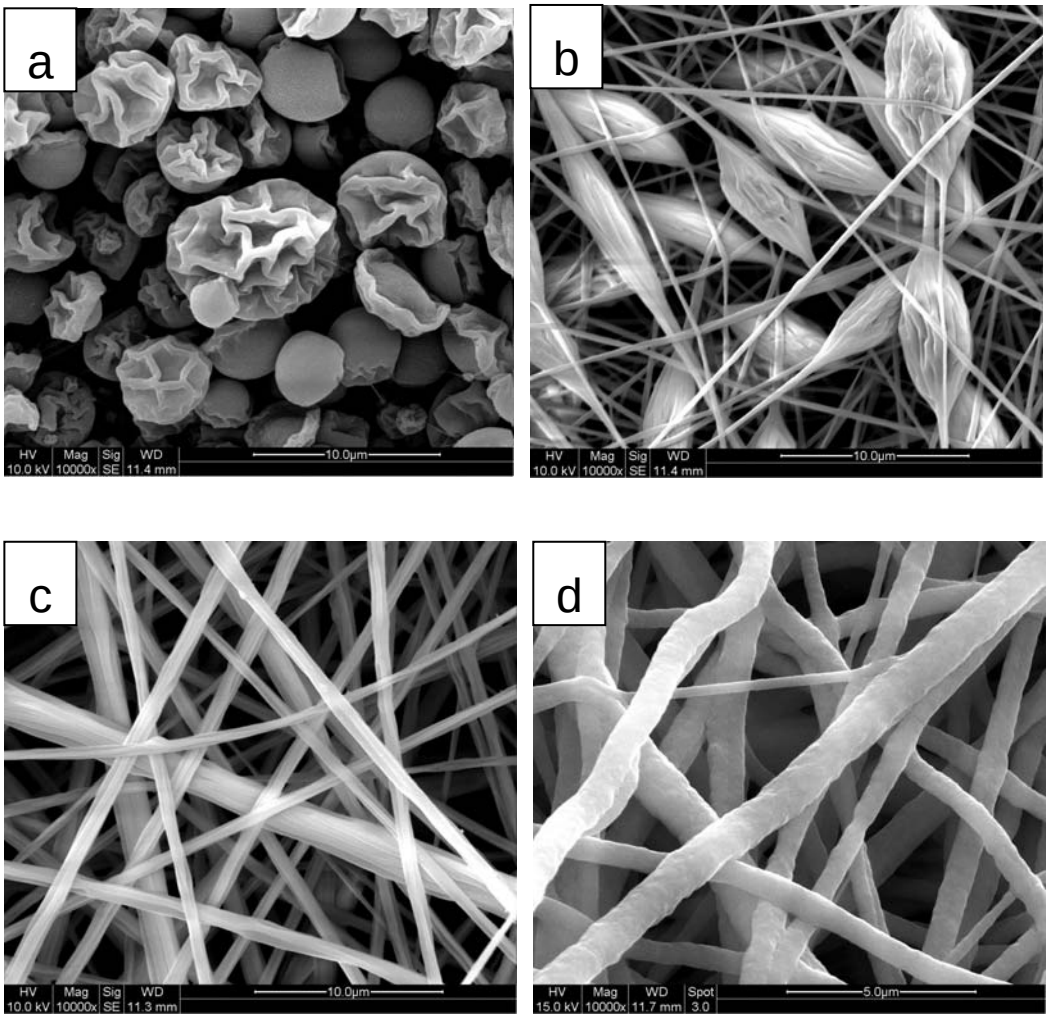

Figure 3.1 Morphologies of fibers electrospun from different solution concentrations with molecular weight of 26,000 g/mol: (a) 10 wt%, (b) 12.6 wt%, (c) 21.2 wt%, (d) 25 wt%.

For concentration 10 wt%, structures consisting only of beads were obtained [Figure 3.1 (a)]. Further increase in concentration to 12.6 wt% resulted in a continuous structure in which all beads were connected by fibers [Figure 3.1 (b)]. This concentration is estimated as entanglement concentration c_e, below which the amount of chain entanglement was negligible. And above this concentration, the occurrence of beads diminished and their shape became more spindle-like until complete fibers [Figure 3.1 (c)] were formed at 21.2 wt%. Thus c_e is the minimum concentration required for the formation of beaded fibers, whereas 2–2.5 times c_e may be required for the formation of bead-free fibers, which is consistent with previous results [46].

Fused structures was observed for extremely high concentrations (C=25 wt%) [Figure 3.1 (d)], indicating incomplete evaporation of the solvent as the solution jet reached the collector. This observation suggests that two competing factors may contribute to the complete evaporation of the solvent. As the fraction of solvent in the solution is increased, the time it takes for complete evaporation is extended beyond the "flight time" thereby leaving fused structures. On the other hand, the formation of a skin (often observed for high concentration) may retard solvent evaporation, as the solvent molecules diffuse much more slowly within the dense skin. Based on these transitions, it can be concluded that for M_w 26,000 g/mol, the onset of incipient fiber formation occurs at C=12.6 wt % and bead-free fibers are stabilized for C>21.2 wt%., which correspond to the onset of fibers from beads and a completely fibrous structure starts to be stabilized.

3.3.2 Molecular weight effects on bead-fiber transition

The bead-fiber transition is also effected by molecular weight. The reduction in polymer molecular weight significantly increased the concentrations at which morphological transitions took place. For Mw =19,300 g/mol, a bead-only structure was obtained for concentrations as high as 18.4 wt % [Figure 3.2 (a)]. Nevertheless, continuous structures began to form upon increasing the concentration to 20 wt% [Figure 3.2 (b)]. The formation of fibers for low-molecular weight solutions may be attributed to the rapid solidification of the jet. For concentrated solutions (C>22 wt%), evaporation of a small amount of solvent may lead to immediate skin formation. This will be discussed in the next chapter.

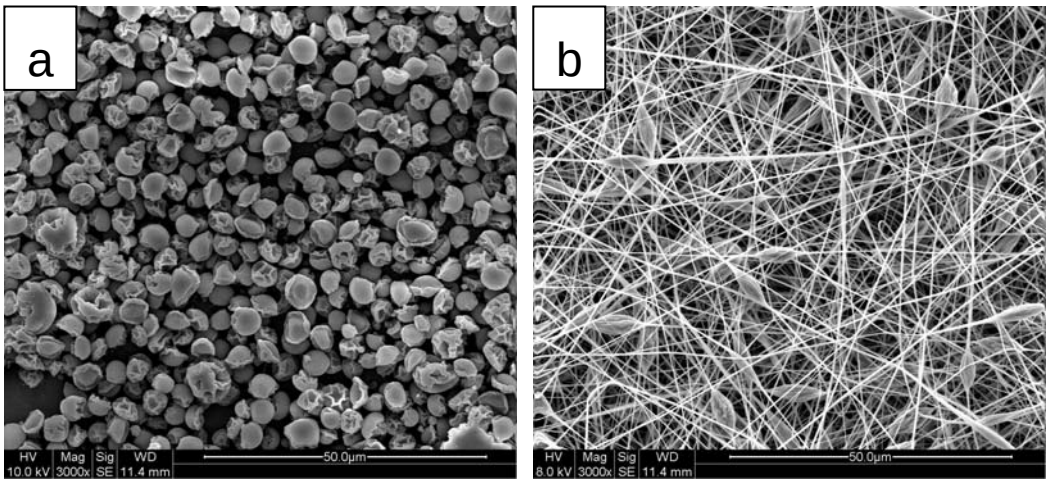

Figure 3.2 Morphologies of fibers electrospun with molecular weight of 19,300 g/mol: (a) 18.4 wt%, (b) 20 wt%.

3.3.3 Applied voltage effects on bead-fiber transition

It should also be noted that a change in the electric field strength may shift the

bead-fiber transition. To illustrate this point, a solution with a concentration slightly below the transition concentration 12.6 wt% was electrospun at a voltage of 10 and 30 kV [Figure 3.3 (a) and (b)]. It is apparent that the bead elimination from beaded fibers when the voltage is increased. The absence of beads in Figure 3.3 (a) may be a result of the increased extensional force in the jet induced by increased electric field. So all the examination of the variation of material properties were conducted at a fixed applied voltage 10 kV.

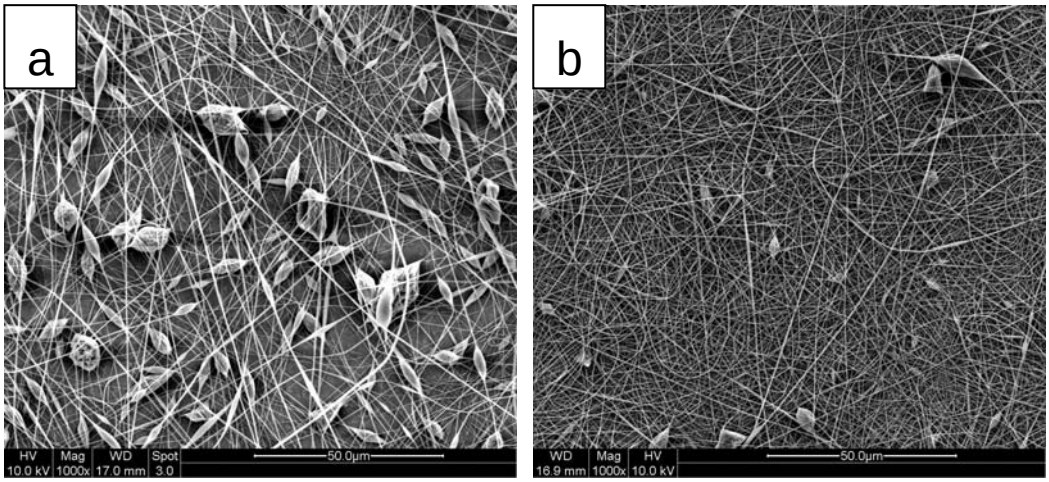

Figure 3.3 Morphologies of fibers electrospun at different applied voltages: (a) 10kV, (b) 30kV.

3.3.4 Anionic surfactant (PDDPPDT) effects on bead-fiber transition

It has been shown that upon electrospinning polysulfone solution of 12.6 wt%, bead-on-fiber structures emerged in the spun fibers. When a small amount of PDDPPDT was added in the polymer solution, the same electrospinning process produced non-beaded fibers. The addition of the surfactants leads to bead-free and

homogeneous fibers. No isolated beads and bead-on-fiber structures were found. The surfactant was so effective that a concentration as low as 0.001 mM was enough to prevent the formation of the beaded fibers [Figure 3.4 (a)].

When the concentration of surfactant was larger than 3 mM, the conductivity of the polymer solution reached a very high value. Long and branched fibers were observed [Figure 3.4(b)], indicating a strong repulsion.

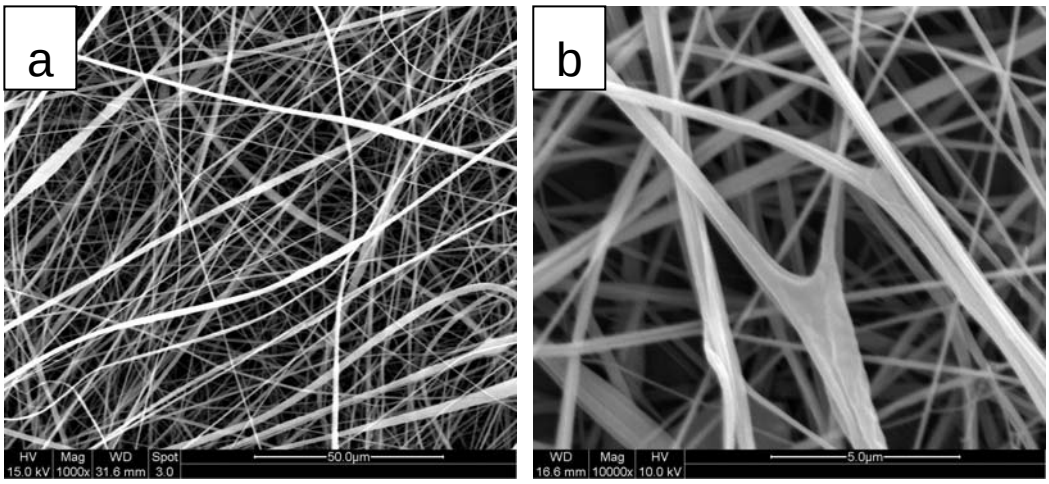

Figure 3.4 Morphologies of fibers electrospun with different concentration of surfactant: (a) 0.001 mM, (b) 3 mM.

The conductivity of the polymer solution was largely improved with increase in the concentration of PDDPPDT. The conductivity value was increased by 100 µS/cm, when the concentration of PDDPPDT was changed from 0.003 to 30 mM [Figure 3.5]. Increasing the solution conductivity suggested that the net charge density of the jet was increased [44]. The whipping instability was thus enhanced and the jet was stretched under the stronger force, resulting in the exhaustion of any bead-like fluid in the whipping process.

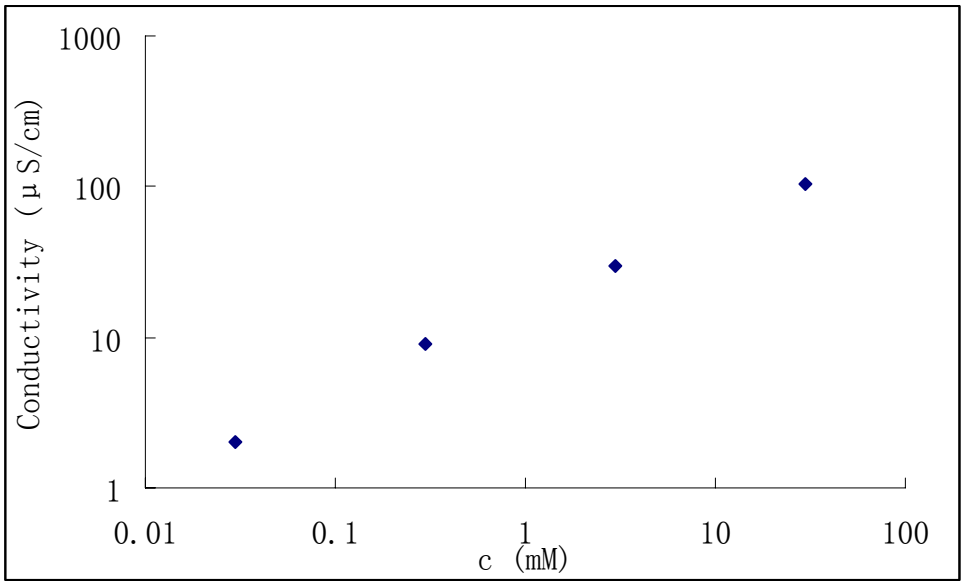

Figure 3.5 Conductivity of electrospinning solutions with different concentration of surfactant.

Further increasing the concentration of surfactant led to a larger charge repulsion that could result in stretching the thread thinner. This result confirmed that the effect of anionic surfactants on the whipping process came from the ionic nature.

The effects of the surfactants on the solution viscosity and the surface tension were also studied. It was found that the addition of anionic surfactants did not affect the solution viscosity. For a 20 wt% polysulfone solution, the viscosity value was about 14.24 cp. This value only fluctuated within the range of experimental error when the concentration of PDDPPDT was changed within 0.003–30 mM. The effect of the surfactant on the surface tension is shown in Figure 3.6. PDDPPDT led to a slight decrease in the surface tension, by 2 dyn/cm, when its concentration was increased from 0.003 to 30 mM.

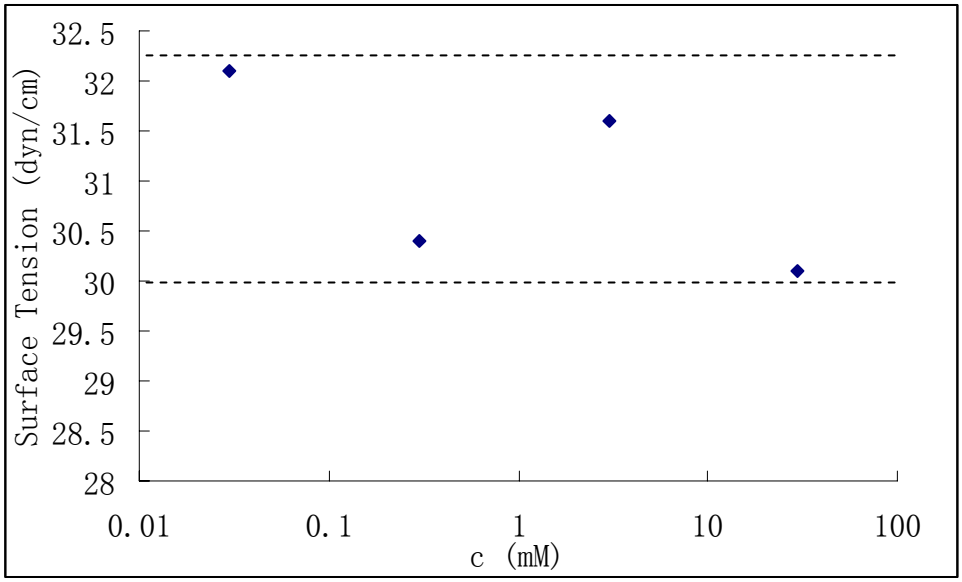

Figure 3.6 Surface tension of electrospinning solutions of 20 wt% with different concentration of surfactant.

3.4 Discussion

3.4.1 Rayleigh instability

The formation of bead and the bead-on-fiber has a lot in common with the phenomenon of laminar jet breakup due to surface tension [49-51]. A Newtonian liquid jet breaks into droplets due to the Rayleigh instability driven by the surface tension. On the contrary, a viscoelastic jet tends to take longer time to break up or does not break up at all, forming a beaded fiber structure or preserving its uniformity. The build up of the extensional stress stabilizes the jet and retards or arrests the Rayleigh instability. This extensional stress in the jet determines the final breakup mechanism [51]. Regardless whether the electrified jet consists of a Newtonian fluid or a viscoelastic fluid, if the Rayleigh break-up instability is not suppressed, the jet can result in a 'bead-on-fiber' structure and ultimately breaks

up into beads. The Rayleigh instability can be slowed down or suppressed by the viscoelastic behavior of the fluid jet.

3.4.2 Competition between Rayleigh instability and elastic response

One way to quantify the competition between the Rayleigh instability growth and the elastic response is to compare the respective time scales. The elastic response of a polymer solution can be described by its relaxation time, λ_p. It was determined by a capillary breakup extensional measurement of the time evolution of the diameter at the mid-point of a fluid filament, following the equation $D_{mid}(t) = D_1\left(\frac{D_1 G}{4\sigma}\right)^{1/3} e^{(-t/3\lambda_p)\,52}$, where G is the elastic modulus, σ is the surface tension, D_1 the initial midpoint diameter just after stretching. A filament is stretched under action of the capillary force, and the diameter at the mid-point of a fluid filament $D_{mid}(t)$ is monitored by the digital camera. The time evolution of the diameter at the mid-point of a fluid filament of four systems is showed [Figure 3.7 and Figure 3.8]: polysulfone solutions of 20 wt%, 25 wt%, 20 wt% with 1% PPDPPDT, 20 wt% with 10% PPDPPDT, respectively. The working plate and the digital camera were directly borrowed from a contact angle meter (Visual Contact Angle (VCA) Optima). The surface tension measurements were performed using a tensiometer (Cole Parmer).

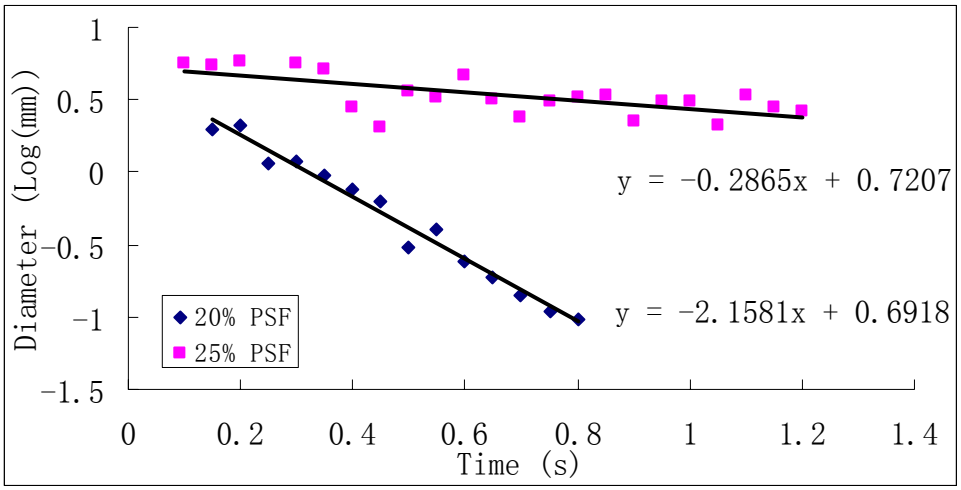

Figure 3.7 Time evolution of the diameter at the mid-point of a fluid filament of 20 wt% and 25 wt% polysulfone solutions

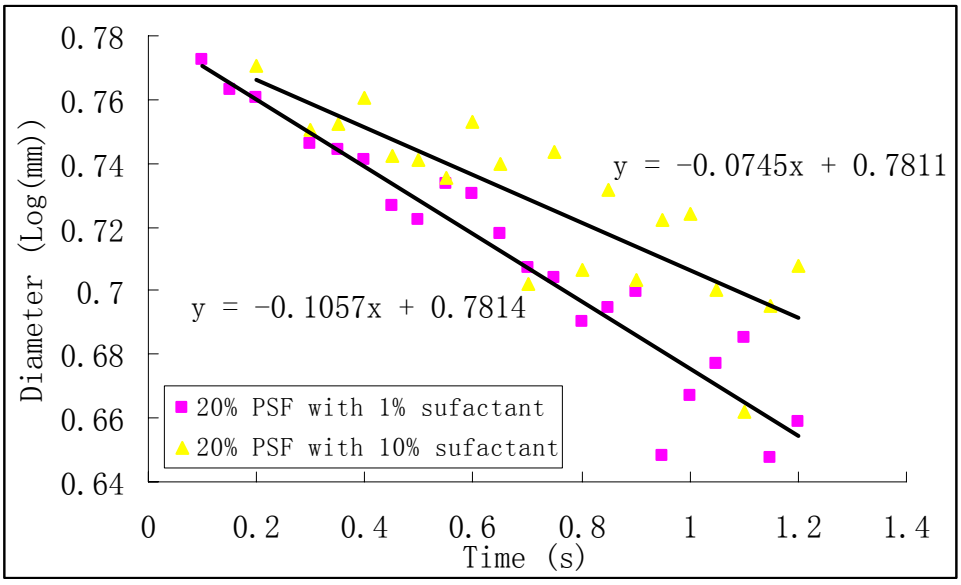

Figure 3.8 Time evolution of the diameter at the mid-point of a fluid filament of 20 wt% polysulfone solutions with 1% and 10% surfactant.

On the other hand, the relevant time scale for the instability growth is the inverse of the instability growth rate. According to Chang, the maximum dimensionless growth rate of a viscoelastic jet ω_{max} corresponding to the fastest growing Rayleigh instability is given by [53], $\omega_{max} = \frac{1}{2\sqrt{2Ca}(1+3S\sqrt{Ca/2})}$, where

$S=1/(1+G\lambda_p/\mu_s)$ is the retardation number, μ_s is the solvent viscosity, $Ca=\rho\upsilon^2/\sigma r_0^2$ is the capillary number, r_0 is the characteristic length, which is taken as the initial radius of the electrified jet, $\upsilon=\mu_s/(S\rho)$ is the characteristic viscosity, ρ is the density.

Yu et al introduced the ratio of the fluid relaxation time and instability growth time [54] $De=\frac{\lambda_p \omega_{max}}{t^*}$, also known as the Deborah number, De. Here $t^*=r_0^2/\upsilon$ is the characteristic time, by which ω_{max} was rendered dimensionless[53]. All of these characteristic parameters are summarized in Table 3.1. Since 10 wt% is the relatively low, it is hard to stretch the tip of solution into filament, its Deborah numbers is estimated to be less than 0.1.

Table 3.1 Characteristic parameters of Rayleigh instability and elastic response in five solution systems

Concentration	10 wt%	20 wt%	25 wt%	20 wt% with 1% surfactant	20 wt% with 10% surfactant
Relaxation time (s)	NA	0.066	0.50	1.35	1.94
Elastic modulus G (Pa)	2.6	2.3	3.3	4.3	4.6
Surface tension (mN/M)	33.4	32.3	30.6	28.6	24.6
Characteristic length (mm)	5.9	5.9	5.9	5.9	5.9
Solvent viscosity (Pa s)	0.00095	0.00095	0.00095	0.00095	0.00095
Retardation number	NA	0.00622	0.00058	0.0001636	0.0001064

Characteristic viscosity	NA	0.00013	0.00141	0.00509	0.00783
Density (kg m^{-3})	1120	1140	1179	1140	1140
Ca	NA	1820	218703	2970104	8159516
ω_{max}	NA	0.00530	0.00045	0.0001284	$7.4*10^{-5}$
De	NA	0.135	0.975	2.535	3.282

For solutions of 20 wt% and 25%, the relaxation time is comparable to the instability growth time, meaning that the capillary forces activate the elastic response, which delays the jet breakup. In this case capillary forces do not break the jet into the droplets like in the case of Newtonian fluids, but gradually squeeze the fluid into the 'beads' connected by highly elastic 'strings'. From this point, only if the instability is completely suppressed by elastic forces or arrested at a very early stage of instability growth (very high De) will the resulting fibers have the appearance of being uniform, which is in contrast to the observation: the nanofiber from solution of 25 wt% is rather uniform. This contradiction indicates that during electrospinning there are other effects suppressing the Rayleigh instability, besides the build up of elastic stress on the jet caused by the extensional deformation. That is the evaporation playing a key role to transfer a uniform jet into a uniform fiber. This will be discussed later in Chapter 3.

3.4.3 Origin of the elastic response: chain entanglements

Examining the conditions employed for all the processes provides a simple explanation: polymer chain overlap is minimal for electrospraying solutions (c/c*).

From the perspective of the electrospraying community, limiting chain entanglements will help generate smaller droplets and more uniform microbeads [55,56]. Chain entanglements within the drop eventually limit the subdivision of these drops. The mechanism for this process is straightforward. As the solvent evaporates, two competing effects occur: (i) polymer concentration increases and entanglements commence, which stabilizes the droplet from further subdivision and (ii) surface charge increases, which overcomes the droplet surface tension providing a driving force for droplet subdivision. A third factor not to be overlooked is heat transfer due to the rapid evaporation of solvent. This effect will also tend to limit the droplet size: as the droplet is cooled, solvent evaporation slows, skin formation stabilizes the droplets, and surface charge no longer increases.

As the polymer concentration is increased ($c \sim c^*$), a mixture of fibers and beads are observed. In this regime, insufficient chain entanglements are present to fully stabilize the jet. In theory, at even higher polymer concentrations ($c > c^*$), increased chain entanglements can temporarily serve to stabilize the electrospinning jet by inhibiting jet breakup. For dry spinning it has been suggested that above a critical dope (polymer) concentration, the dynamic 'short range' network in the spinning solution is converted to a more stable elastically deformable 'long range' network as the solvent evaporates [25,26,57]. In other words, 'spinnable' solutions exhibit elastic properties. In electrospinning, the existence of a similar mechanism may be invoked. An additional consequence of solvent

evaporation is cooling of the jet, which facilitates skin formation and ultimately fiber stabilization.

Chapter 4 Morphology Dependence of Nanofiber on Evaporation

4.1 Introduction

In Chapter 3, the central importance of elastic response of solution in bead-fiber transition has been highlighted. A high degree of elastic response to the extension is observed to arrest the breakup of the jet into fibers by the Rayleigh instability. However, the other two-electric field induced axisymmetric and whipping-instabilities rooted in the charge transportation will not come to an end until the jet is solidified by evaporation. Evaporation plays a key role in the formation of surface morphologies, such as skin and the pores on it.

Recently, Larsen et al.[31] were successful in isolating the effect of evaporation rate by the use of a coaxial gas jacket. Their results show that by controlling the evaporation of volatile solvents, bead-fiber transitions can be induced. It is implied that the formation of stabilizing junctions within the jet of solution by solvent evaporation plays a vital role in determining the resulting polymer structure. In this case, bead-fiber transition is not solely dependent on the entanglement number.

4.2. Experimental section

4.2.1 Materials and measurement

The polysulfone with a molecular weight 26, 000 g mol^{-1} was obtained from Aldrich and used without further purification. Solvents-chloroform, dichloromethane, *N*,*N*-dimethyl formamide (DMF), pyridine were used as received from Aldrich. The concentration of polysulfone solutions of these four solvents were all 20 v/v%.

The morphology of the electrospun fibers was observed under a field emission scanning electron microscope (FE-SEM, Quanta 200F).

4.2.2 Electrospinning

The electrospinning apparatus included a high voltage power supply (ES30P, from Gamma High Voltage Research), a syringe pump (Aldrich) and some accessories. A high voltage was applied to the polymer solution by connecting the electrode with the metal syringe needle. A grounded aluminium sheet was placed about 15 cm away from the tip of the needle. The electrospinning was conducted under the temperature range of 20-25 ℃, and at 1 kV/cm of applied electric field and a polymer flow rate of 1 ml/h.

4.3 Modeling of skin formation

4.3.1 Transport of solvent outside skin

During electrospraying and electrospinning, the jet is commonly larger than the mean free path in air, 0.065 μm. In this continuum regime, evaporation is dominated by the rate at which vapor diffuses away from the surface [58].

The evaporation current (number of molecules per unit area and unit time) is related to diffusivity of solvent vapor in gas $D_g(T)$, $J = D_g(T)\frac{p_g}{kT}\frac{1}{l}$. The solvent partial pressure, p_g, is relate to the volume fraction just below the interface by Henry's law, $\frac{p_g}{p_v(T)} = \psi_u$. The concentration profile of solvent near the surface of skin is showed in Figure 4. l is the thickness of a diffusion layer inside the gas over the nanofiber surface.

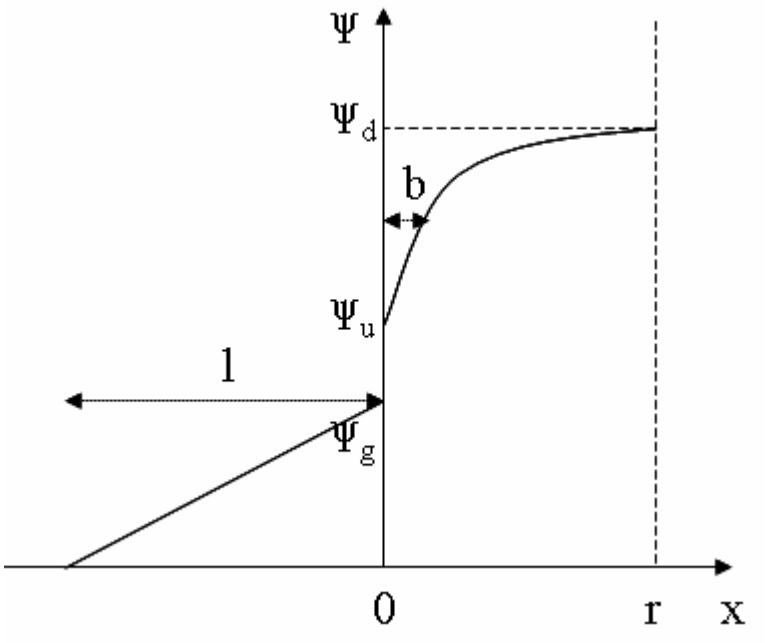

Figure 4.1 Profile of solvent volumetric fraction near the skin of nanofiber (qualitative picture).

The diffusivity $D_g(T)$ is of the order $\upsilon\lambda$, where $\upsilon=(kT/m)^{1/2}$ is the thermal velocity for solvent molecules of mass m, and $\lambda=kT/(a^2p_a)$ is the mean free path in air for solvent molecules of size a in atmospheric pressure. Thus the volumetric evaporation current $a^3 J = \frac{\upsilon a}{l}\frac{p_v(T)}{p_a}\psi_u$

4.3.2 Transport of solvent inside skin

Inside the skin of nanofiber, the diffusion current is at the steady state with the evaporation current, $a^3 J = D(\psi)\frac{d\psi}{dx}$, where $D(\psi)$ is the diffusion coefficient of the solvent in the glassy system. From the free-volume theory, $D(\psi) = D_0 \exp(-q/\psi)$, when solvent effects dominate over temperature effects for diffusion through free volume.

4.3.3 Skin thickness

Now the thickness of skin b can be derived via the slope of the concentration profile near the surface, $b = \psi_u \Big/ \frac{d\psi}{dx}$. Combining with the equations above gives $b = l\frac{p_a}{p_v(T)}\frac{D(\psi_u)}{\upsilon a}$. Supposing for different solvent, the thickness of a diffusion layer inside the gas over the nanofiber surface l, and the volume fraction just below the interface ψ_u are same, $b \propto \frac{m^{1/2}}{p_v(T)a} = Sk$, where Sk is named to skinning number.

4.4 Results and discussion

4.4.1 Results

Polysulfone solutions of the same concentration but different solvent were electrospun in the same processing conditions. The relevant parameters of solvents are listed in Table 4.1.

Table 4.1 Parameters of solvents and characteristic number of skinning of four electrospinning solutions.

Solvents of polysulfone solution (20 v/v%)	Vapour pressure $p_v(T)$ (kPa)	Molecular size a (A)	molecular weight m	Sk
chloroform	21.2	4.72	119.38	0.52
dichloromethane	47.4	4.30	84.93	0.19
N,N-dimethylformamide	0.5	4.90	73.09	17.1
pyridine	4.1	4.85	79.1	4.45

When Sk<1, the nanofiber is ribbon-like with porous skin [Figure 4.2 (a) and (b)]. When Sk~10, the nanofiber has wavy skin with relative small wavelength and small amplitude compared with diameter of nanofiber [Figure 4.2 (c)]. When Sk is between these two limits, the surface has rather significant ridge-valley morphology on the longitude direction [Figure 4.2 (d)].

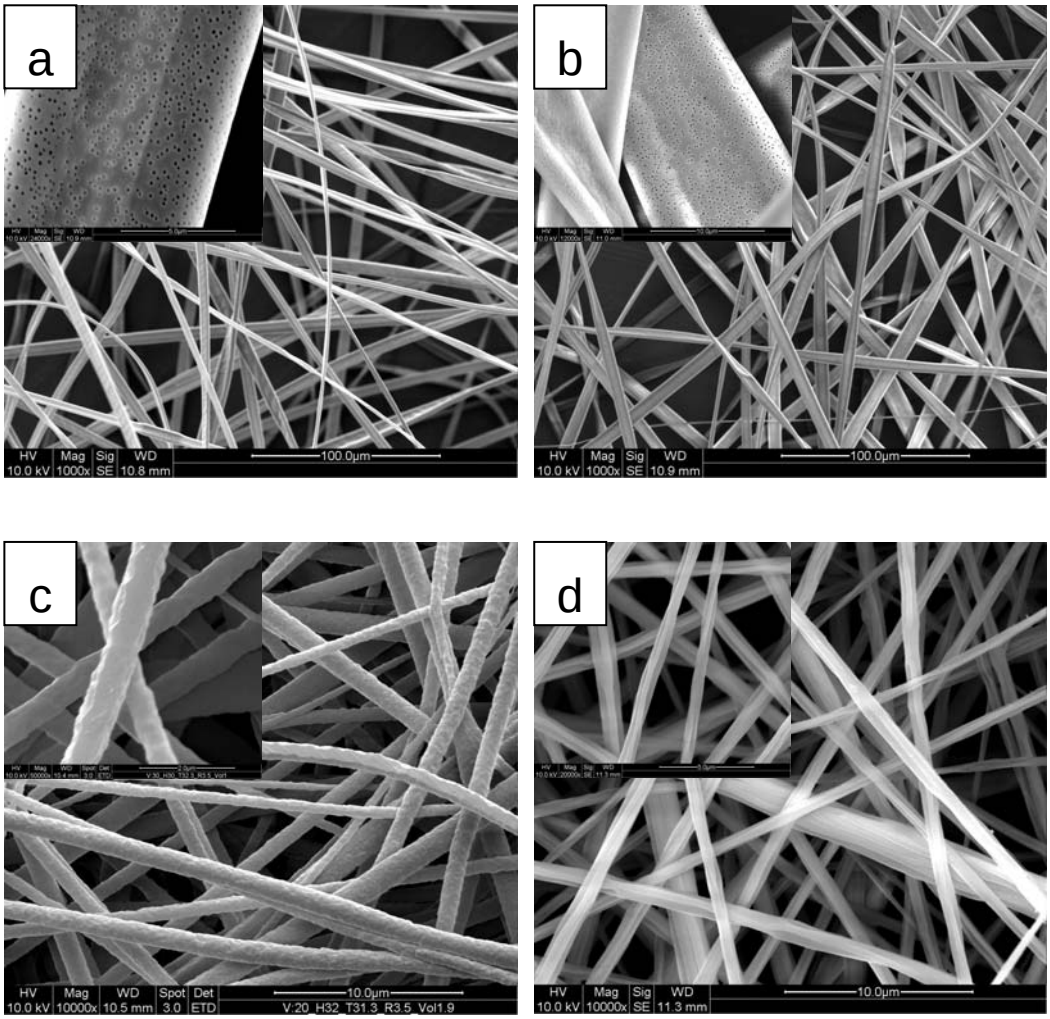

Figure 4.2 Morphologies of fibers electrospun from solutions of four solvents: (a) chloroform, (b) dichloromethane, (c) DMF, (d) pyridine.

4.4.2 Skin formation during evaporation

The different morphologies of nanofibers can be explained with thin shell theory. When the skin of nanofibers is treated as a planar elastic sheet, typical stretching and bending energies per unit area scale as $E_s \sim Yb\zeta^4/l^4$, $E_b \sim Yb^3\zeta^2/l^4$ [59], respectively, where Y is the Young's modulus, b is the thickness of skin, ζ is the magnitude of the out-of-plane displacement, and l is characteristic length of skin. Since the ratio between the two energies is $E_s/E_b \sim (\zeta/b)^2$.

For the case of Sk<1, the skin is rather thin. For instance, using the general form for D(ψ), $D(\psi) = D_0 \exp(-q/\psi)$ with q=1 and ψ*=0.2. Taking l=0.1 mm, p_a/p_v=5, and $D_0/a\upsilon = 10^{-3}$, we arrive at b=14 nanometers. Moreover, the thin skin forms accompany with contraction. Following the ideas of Leibler and Sekimoto [60], we believe that a swollen solid is formed as soon as ψ_u reaches ψ*, and at a later time, this solid is deswollen, with ψ_u decreasing down to ψ*/q. The volume of the entanglement network decreases, but its horizontal dimensions have to remain the same. Thus, there is a tensile stress in the thin skin, as explained in Figure 4.3.

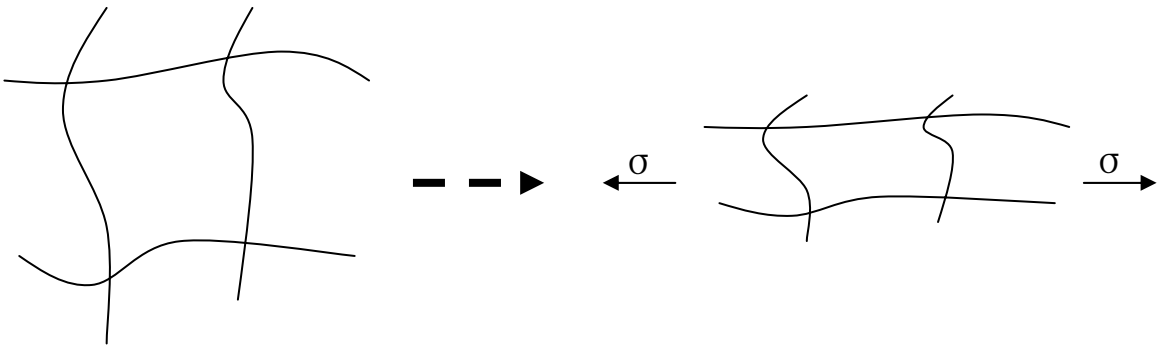

Figure 4.3 Tensile stress induced by volume decreasing.

The overall contraction ratio is of order $\theta = \psi^* - \psi^*/q \cong \psi^*$. With the usual values of ψ*=0.2, this should be sufficient to induce ether plastic deformation or fracture in the skin. It is analogous to a thin soap film that is stretched forming holes on it. Thus the outer surface of the skin exhibits a network of defects.

For the case of Sk~10, the skin is rather thick. The bending energy is much larger than the stretching energy, leading a small out-of-plane displacement. So the fiber

electrospun in DMF solution produce rather smooth surface.

For the case of Sk in median range, the bending and stretching energies compete. It is known that at the top of ridge and bottom of valley stretching energy is rather high, while on the other parts of the surface bending energy dominates. Many applications of nanofiber need the solvent neither of very high volatility (producing large diameter, or blocking the needle), nor of too low volatility (fusion between fibers), that is why in most case it is very hard to achieve nano-scale smooth surface on electrospun fiber.

4.4.3 Other effects during evaporation

Evaporation models of multi component nanofibers require solving the equations for heat and mass transfer at the nanofiber-gas interface as well as the diffusion through the liquid and convective diffusion of the solvent vapor in air. Diffusion through the liquid is generally orders-of-magnitude slower than diffusion through air suggesting the presence of concentration gradients within the fiber. This is confirmed by calculating the Biot number, Bi, which is the ratio of the time scale for self-diffusion in the liquid to the time scale of convective diffusion of the solvent molecules in air. The Biot number for the evaporation of DMF from a pure fiber is given by $\mathrm{Bi} = \frac{d_f k_c}{2D_g}$, where k_c represents the mass transfer coefficient under Stokes flow and is given by $k_c = \frac{D_g}{2a}\left[0.92 + 0.991(\mathrm{Sc}\,\mathrm{Re})^{1/3}\right]$ [61]. Re is the Reynolds number and Sc is the Schmidt number. For DMF, $D_g = 0.13$ cm^2 s^{-1}, Sc

= 1.13, and Re ~ 0.2 at the terminal settling speed of a 400 nm diameter fiber. As a result, Bi ~ 50 indicating the time scale of internal diffusion is significantly greater than the time scale of external, convective diffusion.

As a result, models of multi-component evaporation in nanofiber can employ simplifying assumptions. For the volatile solvents, quasi-steady state models approximate the evaporation dynamics. In quasi-steady state evaporation, fibers exposed to air initially undergo a period of unsteady evaporation while the surface temperature decreases to an equilibrium value [62]. At the equilibrium temperature depression, a binary fiber evaporates at a "constant composition mixture" [63]. In other words, the composition of the fiber is said to be in a quasi-steady state. The rate of evaporation in this state is proportional to the fiber surface area.

Chapter 5 Bead Growth on Nanofiber Induced by Surfactant

5.1 Introduction

Due to the fast evaporation of solvent during electrospinning discussed in Chapter 4, the instabilities discussed in Chapter 3 are frozen, showing unique structures on nanofiber, such as bead-on-fiber. The mechanism of bead-fiber transition has been discussed for the purpose of depressing bead. The most straightforward strategy is to control of operating conditions during electrospinning, such as flow rate, temperature, gas environment, etc. On the other hand, to solve the high-pressure-drop problem of dense nanofiber membrane as filtration medium, a novel idea is introducing bead to increase the space between the nanofibers. A new methodology is developed to grow bead from nanofiber: when nanofibers are placed in a vapor of small molecules, beads are introduced on nanofibers.

A possible mechanism can be explained as follows: sorption and swelling of the small molecules happen first in nanofiber. Since the diffusivity of small molecules such as CEES is of the order of 10^{-15} m^2s^{-1} at room temperature [64], the characteristic time needed for CEES to swell nanofiber of diameter of 100nm is around 1 min, which is much shorter than that of growth of beads. Then the oriented and stretched polymer chains start to coil, which act like springs applying elastic stress along the longitudinal direction of nanofiber. This elastic stress

competes with capillary pressure due to the surface tension. Once the elastic stress wins, the polymer chains are squeezed into certain domain along the nanofiber, forming beads connected by thin filaments.

5.2. Experimental section

5.2.1. Materials and measurement

The polysulfone and anionic surfactant PDDPPDT were the same as in Chapter 3. Pyridine was used as received from Aldrich. The polysulfone solution used pyridine as the solvent, and the concentration of polysulfone was 18 wt%.

5.2.2 Electrospinning

The electrospinning apparatus were described in Chapter 2. Two solutions-18 wt% polysulfone in pyridine with and without 0.5 wt% surfactant PDDPPDT were electrospun into membrane. The electrospinning was conducted in the same conditions: temperature range of 20-25 ℃, 18% humidity, and at 1 kV/cm of applied electric field and a polymer flow rate of 0.5 ml/h, except where specifically indicated.

5.2.3 Sorption

The membrane samples were cut into circular pieces (with radius of 1cm) and evacuated at $p<10^{-5}$ mbar until any significant weight change has ceased, and then put into the sealed cell with nitrogen gas saturated by CEES vapor and/or water

vapor. The temperature of the cell was held constant by a water bath at 303K. The gravimetric measurements were carried out using an electronic microbalance (XT220A Precisa).

5.3 Modeling of growth of bead

The growth of the bead from nanofiber is modeled in Appendix in the frame of hydrodynamic incorporated with molecular-dynamic model. The necessary parameters are summarized in Table 5.1. Among them, the elastic constant of the coiled polymer chain is not available in literature. However, by a simple shooting method of this parameter, the numerical results of the ratio of semi-major and semi-minor radii of beads can be calculated in the same time range as the experiments results. Then an iterative least square comparison between the numerical and experimental results was taken to optimize the value of this parameter. With the knowledge of these parameters one can gain a deeper insight on how the bead grows.

Table 5.1 Summary of parameters for modeling growth of beads

	18% polysulfone: pyridine	18% polysulfone: pyridine with 0.5% surfactant
radius of the undisturbed nanofiber a_0 (m)	$3*10^{-6}$	$3*10^{-6}$
coefficient of surface tension α (kgs^{-2})	$7*10^{-2}$	$5*10^{-2}$

Flory radius r (m)	10^{-7}	10^{-7}
number of Kuhn segments N	$2.36*10^{4}$	$2.36*10^{4}$
perturbation wavelength l	$9a_0$	$9a_0$
elastic constant of the coiled polymer chain k (kgs^{-2})	$9.22*10^{-5}$	$2.58*10^{-3}$
viscosity μ ($kgm^{-1}s^{-1}$)	$3*10^{-3}$	10^{-1}

5.4 Results and discussion

5.4.1 Results

The growth of beads was monitored by imaging with FE-SEM. The semi-major and semi-minor radii of beads were measured for a series of time increments until an equilibrium shape of bead is reached. The ratio of semi-major and semi-minor radii of beads is plot with sorption time in Figure 5.1 and Figure 5.2.

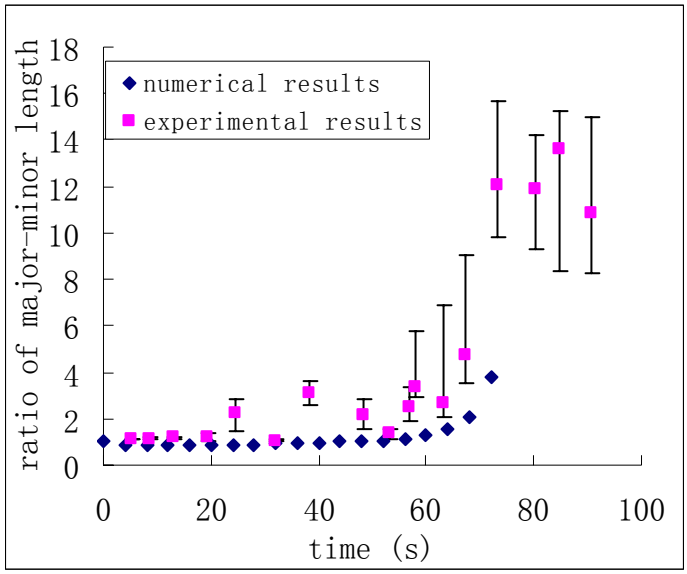

Figure 5.1 Time evolution of the ratio of semi-major and semi-minor radii of

beads, from 18 wt% polysulfone/pyridine solution.

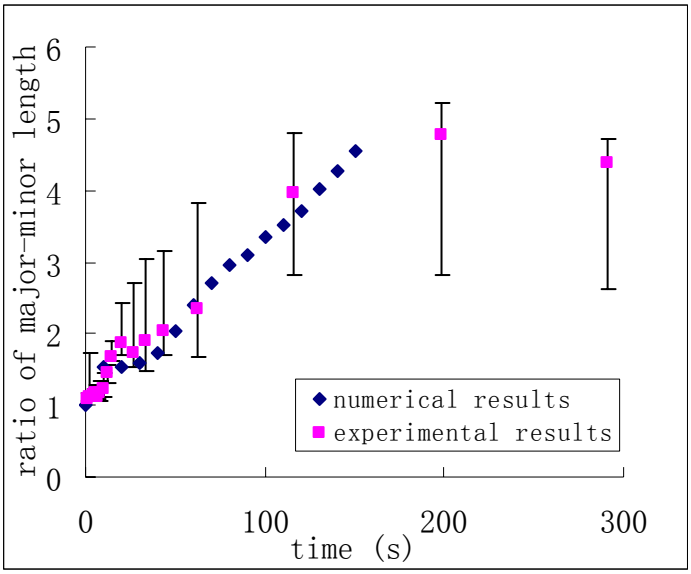

Figure 5.2 Time evolution of the ratio of semi-major and semi-minor radii of beads, from 18 wt% polysulfone/pyridine solution with 0.5 wt% surfactant PDDPPDT.

5.4.2 Relaxation mechanism of bead growth

The determining parameters of bead growth on nanofiber are the relative initial elongation of a polymer chain, $L=L_{xx}(t=0)/r^2$, the volume fraction filled with the polymer chains, $\varphi=4\pi nr^3/3$, and the ratio of the initial modulus of elasticity of a polymer chain to the capillary pressure in the nanofiber, $\tau=ka_0/6\pi r\alpha$. These three parameters are clustered as beading number $Be=9\varphi\tau L/8$, which is the ratio of the elastic energy stored at the initial time in the nanofiber to the surface energy of the nanofiber and therefore characterizes conveniently the relative importance of the elastic and capillary forces.

We note that $Be=2.35*10^{-3}\varphi L$ for the chosen values of the parameters in the

second column of Table 5.1. For φ=0.419, which corresponds to the comparatively high polymer concentration, $Be=10^{-3}L$.

For nanofiber mixed with surfactant, due to the relaxation by interaction with surfactant, it may be expected that polymer chain at smaller values of the relative initial elongation L, of the order of several units or even tens of the elastic stresses. As showed in Figure 5.3 (a) (L=2.5), it will have a weak influence on the initial stage in the growth of the perturbations. In the late stage, instead of rapid breaking of the bridges between the droplets, a beaded structure is formed fast and stabilizes. Indeed, the growth dynamics of the axisymmetric perturbations is similar to the picture of the capillary breakup of a jet of Newtonian fluid.

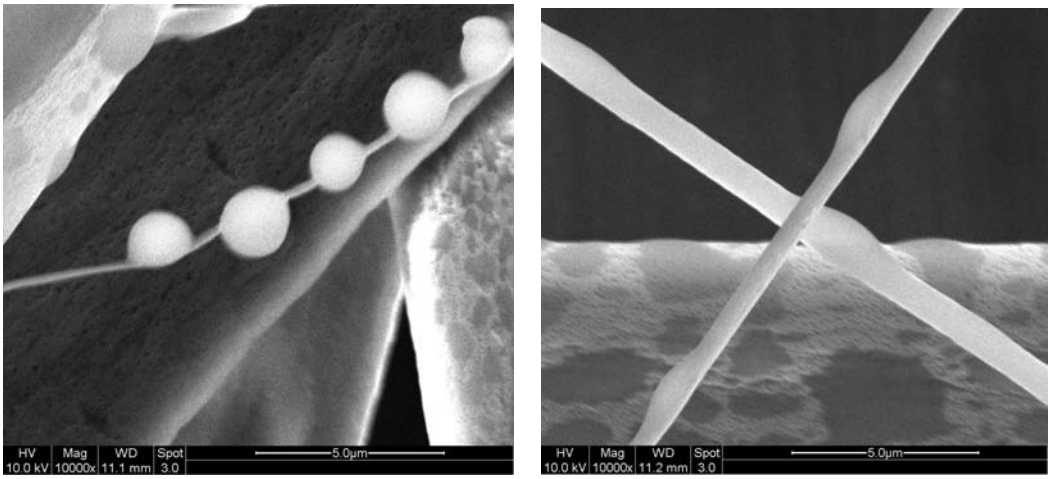

Figure 5.3 Morphologies of nanofiber electrospun: (a) with and (b) without surfactant, after sorption of CEES vapor.

While for nanofiber without surfactant, the increase in the initial elongation L is rather high, to the value 10^2, giving Be~1. At the same time, the elastic stresses already begin to influence the initial stage of the development of the capillary

perturbations. After rapid establishment of self-consistency of the initial perturbations, the nanofiber surface hardly evolves [Figure 5.3 (b)]. There is only partial relaxation of the initial elastic stresses. The growth in this case is slower than the case with L = 2.5.

5.4.3 Further simplification

From the above analysis, the growth of bead can be clearly related to the ratio of the elastic energy to capillary energy. For nanofiber mixed with surfactant, this ratio is on the order of 10^{-3}, meaning the surface tension dominates. So in the later stage of bead growth it is simplified as a liquid droplet growth on a fiber, driven by capillary pressure.

With an initial perturbation, the resulting gradient in capillary pressure causes flow from the neck toward the bulb, causing flow out of the thinning neck. For a long time after the onset of the flow, a minimum radius of neck is reached, and a microthread forms. In the absence of surfactant, the microthread would continue to thin. The presence of surfactant, however, gives rise to a force that acts as a brake on the further thinning. This is because of the flow during the initial stages of pinching, a gradient in surfactant concentration or surface tension exists. Consequently, the surface tension-gradient-induced Marangoni stress is predominantly negative and acts to slow down the evacuation of fluid out of the neck into the bulbous region. This axisymmetric conformation of droplet on fiber is quasi-equilibrium, that it will be stable for long time.

Due to Young-Laplace Equation, a net capillary pressure change makes axisymmetric droplet unstable, and induces perturbative movement of contact line. Under the condition of conservation of volume, the surface of droplet deforms with one curvature increased and the other decreased to minimize its surface energy, giving the non-axisymmetric configuration of beads in Figure 5.4.

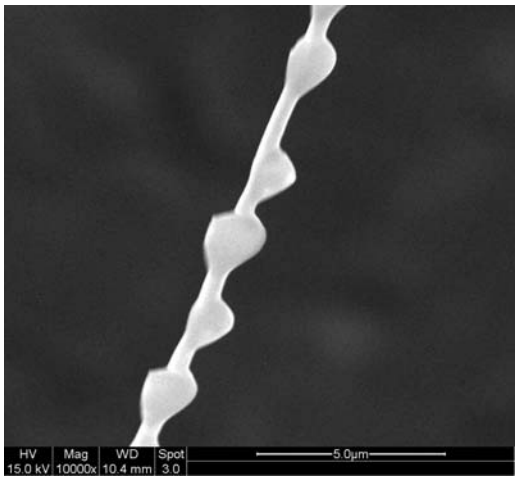

Figure 5.4 Non-axisymmetric beads

To analyze the dynamics of non-axisymmetric growth, considering the perturbation of Young-Laplace Equation,

$$\delta(\Delta P) = \gamma(\delta R_1^{-1} + \delta R_2^{-1}) + \delta\gamma(R_1^{-1} + R_2^{-1})$$
$$= \gamma\left(\frac{n^4 - 4n^3\cos\theta + 4n^2 - 1}{n^2(n^2-1)^2} - \frac{1}{n^2}\right) + \delta\gamma\left(\frac{n^2 - 2n\cos\theta + 1}{n(n^2-1)^2} - \frac{1}{n}\right),$$

where θ is the contact angle, and $n = \frac{x_2}{x_1}$, x_1 is the radius of fiber, x_2 is the radius of bulbous region. Both θ and n together determine the shape the droplet.

If neglecting the change of surface tension with shape transformation, the second term of this equation is vanished. When $\delta(\Delta P)=0$, the shape is considered stable, θ and n satisfies $2n^3\cos\theta-3n^2+1=0$, which is given in Figure 5.5.

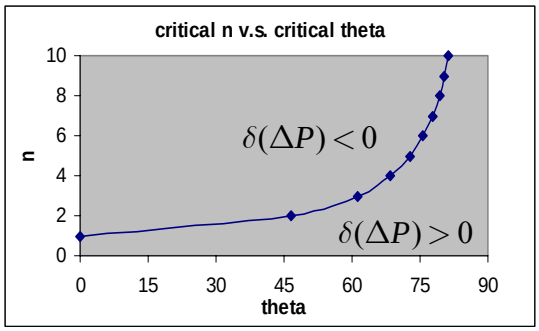

Figure 5.5 Critical shape of beads by balance of capillary pressure and hydrostatic pressure

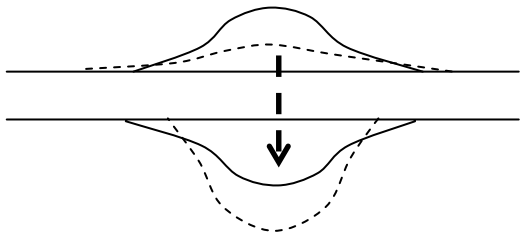

Figure 5.6 Flow of fluid inducing non-axisymmetric beads

If $\delta(\Delta P)<0$, there will be a flow of fluid from the part of lower average radius to the part of higher average radius (following the arrow in Figure 5.6). This flow will once again decrease R_2 and since R_1 is also less than its initial unperturbed value, the flow is sustained, and the contact angle increases with time, until a clamshell shape droplet forms.

Furthermore, if the relation between the surface tension change and shape deformation is derived at the molecular level, the curve in Figure 5.5 could be

modified by considering the second term in the perturbative Young-Laplace equation.

Chapter 6 Conclusions and Future Work

6.1 Conclusions

The presented work was carried out with the motivation of developing HNIN for functional applications. The objective of the work was to fundamentally investigate the morphology dependence of nanofibers and nanoparticles on processing and post-treatment conditions. Hence, from presented work the following conclusions can be derived:

During processing, Rayleigh instability driven by surface tension tends to break fluid filament into droplets, while the extensional stress built up by elasticity stabilizes the fluid filament. The competition between the Rayleigh instability and elastic relaxation is quantified in Deborah number, which is the ratio of the fluid relaxation time and instability growth time. When De>1, the solutions mostly can be electrospun into bead-free nanofibers. To achieve enough elasticity of fluid filament, critical amount of polymer chain entanglements is needed. The chain entanglement increases with increase in the concentration of solution and molecular weight of polymer.

Whereas De>1 is only one of the necessary conditions for bead-free nanofibers, because it only considers the hydrodynamic constraints. In some cases of De<1, the formation of bead-free nanofibers was also observed. One reason is that, as the solvent evaporates, surface charge increases, which adds extra electric stress along

the surface to overcome the surface tension. So with higher applied voltage or conductivity of solution, the bead-fiber transition happens at a lower concentration. This indicates that the electric stress helps extensional stress built up by elasticity to compete with Rayleigh instability.

Another reason for obtaining bead-free nanofibers when De<1 is that as the solvent evaporates, skin forms with decreased volume, which induces in-plane tensile stress. The tensile stress competes with Rayleigh instability, and prefers fibers to beads. The skin thickness, as well as morphology of nanofibers, is characterized by skinning number, which highly depends on the volatility of solvent. When Sk<1, the nanofiber is ribbon-like with porous skin; when Sk~10, the nanofiber has wavy skin with relative small wavelength and small amplitude compared with diameter of nanofiber. When Sk is between these two limits, the surface has rather significant ridge-valley morphology on the longitude direction.

The beads not only can be manipulated by controlling the processing parameters and solution properties, but can also be introduced on nanofibers by post-treatment in CEES vapor. With the sorption and swelling with CEES, the stretched and oriented polymer chains start to coil, which act like springs applying elastic stress along the longitudinal direction of nanofiber. The competition between the elastic stress and surface tension is characterized by beading number, which is the ratio of the elastic energy stored at the initial time in the nanofiber to the surface energy of the nanofiber. For nanofiber mixed with surfactant, Be is on

the order of 10^{-3}, meaning the surface tension dominates. So the bead growth can be simplified as a liquid droplet growth on a fiber, driving by capillary pressure.

6.2 Future Works

Based on the results obtained from the present study, the future works for developing HNIN have been suggested.

All of systems in the present study were solutions of PSF which is a common material for filtration applications. Using the methodology provided here, other polymer systems can be investigated for various applications of HNIN. For example, by gradually changing proportion of mixed solvents, the nanofibers can be deposited with morphologies “gradient” layer by layer. Since the morphology of nanofibers effects the differentiation of stem cell, it is possible to induce different cell subsets in a single nanofiber membrane, such as human skin.

Most of systems in the present study were homogeneous solutions. While it is observed that in heterogeneous solutions, bead-fiber transition happens at very high concentration, which leading to failure to get uniform nanofibers, such as polymer solution blended with carbon nanotube for sensor application, and blended with MgO nanoparticles for detoxification application. An in-depth investigation on the sufficient conditions to depress bead in heterogeneous solutions, and also with consideration of the second phase, modification of De, Sk, and Be, are some challenges that would be worthwhile investigating in the future.

References

1. Rayleigh, L. On the equilibrium of liquid conducting masses charged with electricity. *Philosophical Magazine* 1882, *14*, 184-186.

2. Zeleny, J. Instability of electrifield liquid surfaces. *Physical Reviews* 1917, *10*, 1.

3. Taylor, G. I. Distintegration of water drops in an electric field. *Proceedings of the Royal Society of London. Series A* 1964, *280*, 8.

4. Taylor, G. I. *Proceedings of the Royal Society of London. Series A* 1966, *291*, 159.

5. Hines, R. L. J. *Journal of Applied Physics* 1966, *37*, 2730.

6. Tilney, R.; Peabody, H. W. *British Journal of Applied Physics* 1953, *4*, S1.

7. Dole, M.; Mack, L. L.; Hines, R. L.; Mobley, R. C.; Ferguson, L. D.; Alice, M. B. Molecular beams of macroions. *Journal of Physical Chemistry* 1968, *49*, 2240.

8. Yamashita, M.; Fenn, J. B. Electrospray Ion-Source - Another Variation on the Free-Jet Theme. *Journal of Physical Chemistry* 1984, *88* (20), 4451-4459.

9. Yamashita, M.; Fenn, J. B. Negative-Ion Production with the Electrospray Ion-Source. *Journal of Physical Chemistry* 1984, *88* (20), 4671-4675.

10. Wong, S. F.; Meng, C. K.; Fenn, J. B. Multiple Charging in Electrospray Ionization of Poly(Ethylene Glycols). *Journal of Physical Chemistry* 1988, *92* (2), 546-550.

11. Fenn, J. B.; Mann, M.; Meng, C. K.; Wong, S. F.; Whitehouse, C. M. Electrospray Ionization for Mass-Spectrometry of Large Biomolecules. *Science* 1989, *246* (4926), 64-71.

12. Morton, W. J. US705691, 1902.

13. Cooley, J. F. patent US692631, 1902.

14. Formhal, A. patent US1975504, 1930.

15. Norton, C. L. patent US2048651, 1936.

16. Fuchs, N. A.; Petryanov-Sokolov, I. V. Sovient USSR3444, 1938.

17. Simm, W.; Gosling, K.; Bonart, R.; von Falkai, B. Germany GB1346231, 1972.

18. Jacobsen, M. *Chemiefasern/Textilind* 1991, *41*, 36.

19. Doshi, J.; Srinivasan, G.; Reneker, D. *Polym. News* 1995, *20*, 206.

20. Simpson, D. G.; Bowlin, G. L.; Wnek, G. E.; Stevens, P. J.; Carr, M. E.; Matthews, J. A.; Rajendran, S. *Biomacromolecules* 2002, 3, 232.

21. Huang, Z. M.; Zhang, Y. Z.; Kotaki, M.; Ramakrishna, S. A review on polymer nanofibers by electrospinning and their applications in nanocomposites. *Composites Science and Technology* 2003, *63* (15), 2223-2253.

22. Shenoy, S. L.; Bates, W. D.; Frisch, H. L.; Wnek, G. E. Role of chain entanglements on fiber formation during electrospinning of polymer solutions: good solvent, non-specific polymer-polymer interaction limit. *Polymer* 2005, *46* (10), 3372-3384.

23. Gupta, P.; Wilkes, G. L. Some investigations on the fiber formation by utilizing a side-by-side bicomponent electrospinning approach. *Polymer* 2003, *44* (20), 6353-6359.

24. Jun, Z.; Hou, H. Q.; Schaper, A.; Wendorff, J. H.; Greiner, A. Poly-L-lactide nanofibers by electrospinning - Influence of solution viscosity and electrical conductivity on fiber diameter and fiber morphology. *E-Polymers* 2003.

25. Gou, Z. M.; Mchugh, A. J. Two-dimensional modeling of dry spinning of polymer fibers. *Journal of Non-Newtonian Fluid Mechanics* 2004, *118* (2-3), 121-136.

26. Gou, Z. M.; Mchugh, A. J. A comparison of Newtonian and viscoelastic constitutive models for dry spinning of polymer fibers. *Journal of Applied Polymer Science* 2003, *87* (13), 2136-2145.

27. Mckee, M. G.; Elkins, C. L.; Long, T. E. Influence of self-complementary hydrogen bonding on solution rheology/electrospinning relationships. *Polymer* 2004, *45* (26), 8705-8715.

28. Mckee, M. G.; Park, T.; Unal, S.; Yilgor, I.; Long, T. E. Electrospinning of linear and highly branched segmented poly(urethane urea)s. *Polymer* 2005, *46* (7), 2011-2015.

29. Shenoy, S. L.; Bates, W. D.; Wnek, G. Correlations between electrospinnability and physical gelation. *Polymer* 2005, *46* (21), 8990-9004.

30. Stephens, J. S.; Frisk, S.; Megelski, S.; Rabolt, J. F.; Chase, D. B. "Real time" Raman studies of electrospun fibers. *Applied Spectroscopy* 2001, *55* (10), 1287-1290.

31. Larsen, G.; Spretz, R.; Velarde-Ortiz, R. Use of coaxial gas jackets to stabilize Taylor cones of volatile solutions and to induce particle-to-fiber transitions. *Advanced Materials* 2004, *16* (2), 166-+.

32. Boger, D. V. A highly elastic constant-viscosity fluid. *J. Non-Newton Fluid Mechanics* 1977, *3* (1), 87-91.

33. Dontula, P.; Macosko, C. W.; Scriven, L. E. Model elastic liquids with water-soluble polymers. *AIChE Journal* 1998, *44* (6), 1247-1255.

34. Zong, X. H.; Kim, K.; Fang, D. F.; Ran, S. F.; Hsiao, B. S.; Chu, B. Structure and process relationship of electrospun bioabsorbable nanofiber membranes. *Polymer* 2002, *43* (16), 4403-4412.

35. Fong, H.; Chun, I.; Reneker, D. H. Beaded nanofibers formed during electrospinning. *Polymer* 1999, *40* (16), 4585-4592.

36. Son, W. K.; Youk, J. H.; Lee, T. S.; Park, W. H. The effects of solution properties and polyelectrolyte on electrospinning of ultrafine poly(ethylene oxide) fibers. *Polymer* 2004, *45* (9), 2959-2966.

37. Lee, K. H.; Kim, H. Y.; Khil, M. S.; Ra, Y. M.; Lee, D. R. Characterization of nano-structured poly(epsilon-caprolactone) nonwoven mats via electrospinning. *Polymer* 2003, *44* (4), 1287-1294.

38. Yang, Q. B.; Li, Z. Y.; Hong, Y. L.; Zhao, Y. Y.; Qiu, S. L.; Wang, C.; Wei, Y. Influence of solvents on the formation of ultrathin uniform poly(vinyl pyrrolidone) nanofibers with electrospinning. *Journal of Polymer Science Part B-Polymer Physics* 2004, *42* (20), 3721-3726.

39. Eda, G.; Liu, J.; Shivkumar, S. Solvent effects on jet evolution during electrospinning of semi-dilute polystyrene solutions. *European Polymer Journal* 2007, *43* (4), 1154-1167.

40. Wu, X. H.; Wang, L. G.; Yu, H.; Huang, Y. Effect of solvent on morphology of electrospinning ethyl cellulose fibers. *Journal of Applied Polymer Science* 2005, *97* (3), 1292-1297.

41. Hsu, C. M.; Shivkumar, S. N,N-dimethylformamide additions to the solution for the electrospinning of poly(epsilon-caprolactone) nanofibers. *Macromolecular Materials and Engineering* 2004, *289* (4), 334-340.

42. Lee, K. H.; Kim, H. Y.; Bang, H. J.; Jung, Y. H.; Lee, S. G. The change of bead morphology formed on electrospun polystyrene fibers. *Polymer* 2003, *44* (14), 4029-4034.

43. Lee, K. H.; Kim, H. Y.; La, Y. M.; Lee, D. R.; Sung, N. H. Influence of a mixing solvent with tetrahydrofuran and N,N-dimethylformamide on electrospun poly(vinyl chloride) nonwoven mats. *Journal of Polymer Science Part B-Polymer Physics* 2002, *40* (19), 2259-2268.

44. Lin, T.; Wang, H. X.; Wang, H. M.; Wang, X. G. The charge effect of cationic surfactants on the elimination of fibre beads in the electrospinning of polystyrene. *Nanotechnology* 2004, *15* (9), 1375-1381.

45. Gupta, P.; Elkins, C.; Long, T. E.; Wilkes, G. L. Electrospinning of linear homopolymers of poly(methyl methacrylate): exploring relationships between fiber formation, viscosity, molecular weight and concentration in a good solvent. *Polymer* 2005, *46* (13), 4799-4810.

46. Mckee, M. G.; Wilkes, G. L.; Colby, R. H.; Long, T. E. Correlations of solution rheology with electrospun fiber formation of linear and branched polyesters. *Macromolecules* 2004, *37* (5), 1760-1767.

47. Theron, S. A.; Zussman, E.; Yarin, A. L. Experimental investigation of the governing parameters in the electrospinning of polymer solutions. *Polymer* 2004, *45* (6), 2017-2030.

48. Yarin, A. L.; Koombhongse, S.; Reneker, D. H. Bending instability in electrospinning of nanofibers. *Journal of Applied Physics* 2001, *89* (5), 3018-3026.

49. Goldin, M.; Yerushalmi, J.; Pfeffer, B.; Shinnar, R. Breakup of. a laminar capillary jet of a viscoelastic fluid. *Journal of Fluid Mechanics* 1969, *36*, 689.

50. Funada, T.; Joseph, D. D. Viscoelastic potential flow analysis of capillary instability. *Journal of Non-Newtonian Fluid Mechanics* 2003, *111* (2-3), 87-105.

51. Bousfield, D. W.; Keunings, R.; Marrucci, G.; Denn, M. M. Nonlinear-Analysis of the Surface-Tension Driven Breakup of Viscoelastic Filaments. *Journal of Non-Newtonian Fluid Mechanics* 1986, *21* (1), 79-97.

52. Rodd, L. E.; Scott, T. P.; Cooper-White, J. J.; McKinley, G. H. Capillary break-up rheometry of low-viscosity elastic fluids. *Applied Rheology* 2005, *15* (1), 12-27.

53. Chang, H. C.; Demekhin, E. A.; Kalaidin, E. Iterated stretching of viscoelastic jets. *Physics of Fluids* 1999, *11* (7), 1717-1737.

54. Yu, J. H.; Fridrikh, S. V.; Rutledge, G. C. The role of elasticity in the formation of electrospun fibers. *Polymer* 2006, *47* (13), 4789-4797.

55. Festag, R.; Alexandratos, S. D.; Joy, D. C.; Wunderlich, B.; Annis, B.; Cook, K. D. Effects of molecular entanglements during electrospray of high molecular weight polymers. *Journal of the American Society for Mass Spectrometry* 1998, *9* (4), 299-304.

56. Festag, R.; Alexandratos, S. D.; Cook, K. D.; Joy, D. C.; Annis, B.; Wunderlich, B. Single- and few-chain polystyrene particles by electrospray. *Macromolecules* 1997, *30* (20), 6238-6242.

57. Griswold, P. D.; Cuculo, J. A. An experimental study of the relationship between rheological properties and spinnability in the dry spinning of cellulose acetate-acetone solutions. *Journal of Applied Polymer Science* 1974, *18* (10), 2887-2902.

58. Hinds, W. C. *Aerosol Technology: Properties, Behavior, and Measurement of Airborne Particles;* 2nd ed.; John Wiley & Sons, Inc.: New York: 1999.

59. Komura, S.; Tamura, K.; Kato, T. Buckling of spherical shells adhering onto a rigid substrate. *European Physical Journal e* 2005, *18* (3), 343-358.

60. Leibler, L.; Sekimoto, K. On the Sorption of Gases and Liquids in Glassy-Polymers. *Macromolecules* 1993, *26* (25), 6937-6939.

61. Clark, M. M. *Transport Modeling for Environmental Engineers and Scientists;* Wiley Interscience: New York: 1996.

62. Newbold, F. R.; Amundson, N. R. A model for evaporation of a multicomponent droplet. *AIChE Journal* 1973, *19* (1), 22-30.

63. Ray, A. K.; Venkatraman, S. Binary Activity-Coefficients from Microdroplet Evaporation. *AIChE Journal* 1995, *41* (4), 938-947.

64. Rajagopalan, G.; Gillespie, J. W.; McKnight, S. H. Diffusion of reacting epoxy and amine monomers in polysulfone: a diffusivity model. *Polymer* 2000, *41* (21), 7723-7733.

Appendix

To describe the bead growth on nanofibers, we use the dynamical equations in the quasi-one-dimensional approximation. The equations of continuity and momentum in the form

$$\frac{\partial a^2}{\partial t}+\frac{\partial V a^2}{\partial x}=0,\ \ \frac{\partial}{\partial x}\left\{\Sigma_{\tau\tau}a^2+2\alpha a\left[1+\left(\frac{\partial a}{\partial x}\right)^2\right]^{-1/2}\right\}=0 \quad (1.1)$$

Here, t is the time, x is the coordinate along the jet axis, a is the radius of the jet, V is the longitudinal velocity, $\Sigma_{\tau\tau}$ is the longitudinal stress, and α is the coefficient of surface tension. The momentum equation is written down directly in the inertialess approximation, since in what follows we shall concentrate on situations in which the viscous and elastic forces dominate over the inertial forces.

The system (1.1) is closed by specifying the molecular--hydrodynamic rheological model, which adequately describes elongation flows and meets all the invariance and objectivity requirements of formal theology. Using this rheological model, we obtain for a jet in the quasi-one-dimensional approximation the equations

$$\Sigma_{\tau\tau}=3\mu(1+5nr^3K_1)\frac{\partial V}{\partial x}-\alpha\left\{\frac{1}{a\sqrt{1+(\partial a/\partial x)^2}}-\frac{\partial^2 a/\partial x^2}{\sqrt{1+(\partial a/\partial x)^2}}\right\}+nkK_2(L_{\tau\tau}-L_{nn})$$

$$\frac{\partial L_{nn}}{\partial t}+V\frac{\partial L_{nn}}{\partial x}=-K_1L_{nn}\frac{\partial V}{\partial x}-K_2K_3(L_{nn}-\frac{r^2}{3}) \quad ,$$

$$\frac{\partial L_{\tau\tau}}{\partial t}+V\frac{\partial L_{\tau\tau}}{\partial x}=2K_1L_{\tau\tau}\frac{\partial V}{\partial x}-K_2K_3(L_{\tau\tau}-\frac{r^2}{3}),$$

$$K_1=\frac{2L_{nn}+L_{\tau\tau}}{3r^2+2L_{nn}+L_{\tau\tau}},\quad K_2=\frac{Nb}{Nb-\sqrt{2L_{nn}+L_{\tau\tau}}},K_3=\frac{2kr}{6\pi\mu r\sqrt{2L_{nn}+L_{\tau\tau}}}\quad (1.2)$$

Here, μ is the viscosity of the solvent; L_{nn} and $L_{\tau\tau}$ are the normal and axial components of the orientation--deformation tensor; n is the number of polymer chains in unit volume; b is the length of a Kuhn segment; N is the number of Kuhn segments in a polymer chain; $r=b/\sqrt{N}$; k is the elastic constant of the coiled macromolecule

We take l the perturbation wavelength. By virtue of the periodicity of the solution, at any time we have boundary condition: V = 0 at x = 0 and *1/2,* so that integrating the second equation in (l.l) and using the first equation in (1.2), we could find the velocity distribution in the nanofiber. With the velocity the continuity equation in (1.1) was integrated using an explicit approximation scheme. The rheological equations (the last two equations of (1.2)) were integrated using a combined explicit-implicit difference scheme.

Then we get $V=V_0(t)+C(t)\int_0^x f_1(\xi)d\xi-\int_0^x f_2(\xi)d\xi$, where $f_1=\left[3\mu a^2(1+5nr^3K_1)\right]^{-1}$. The integration of the velocity in this equation clearly describes the bead growth with time